

## Article

# Numerical Simulation on the Influence of the Distribution Characteristics of Cracks and Solution Cavities on the Wellbore Stability in Carbonate Formation

Jingzhe Zhang <sup>1</sup>, Rongrong Zhao <sup>1,\*</sup>, Hongyi An <sup>1</sup>, Wenhao Li <sup>1</sup>, Yuxin Geng <sup>2</sup>, Xiangyu Fan <sup>3</sup> and Qianguai Zhang <sup>4,\*</sup>

- <sup>1</sup> Exploration Utility Department, CNPC Southwest Oil and Gas Field Company, Chengdu 610095, China; zhangjingzhe@petrochina.com.cn (J.Z.); anhongyi@petrochina.com.cn (H.A.); liwhao@petrochina.com.cn (W.L.)
- <sup>2</sup> Shanxi CBM Exploration and Development, CNPC Huabei Oil Field Company, Changzhi 046000, China; ggynl1999@163.com
- <sup>3</sup> School of Geoscience and Technology, Southwest Petroleum University, Chengdu 610500, China; 199931010004@swpu.edu.cn
- <sup>4</sup> Petroleum Engineering School, Southwest Petroleum University, Chengdu 610500, China
- \* Correspondence: zhao\_rr@petrochina.com.cn (R.Z.); qgzhang@swpu.edu.cn (Q.Z.); Tel.: +86-028-8303-7050 (Q.Z.)

**Abstract:** The development of cracks and solution cavities in carbonate reservoirs can notably reduce the rock's mechanical properties, leading to a severe wellbore collapse problem during drilling operations. To clarify the influence of the characteristics of cracks and solution cavities on the wellbore stability in the Dengying Formation carbonate reservoir in the Gaoshiti–Moxi area of Sichuan, the mechanical properties of carbonate rock were analyzed. Then, the influences of the attitude and width of cracks, the size and quantity of solution cavities, and their connectivity on wellbore stability were studied using FLAC3D 6.00 numerical simulation software. Our results show the following: (1) The cracks and solution cavities in the Dengying Formation carbonate rock cause significant differences in the rock's mechanical properties. (2) The equivalent drilling fluid density of collapse pressure ( $\rho_c$ ) considering the effects of cracks and solution cavities is 6.4% higher than without these effects, which is in good accordance with engineering practice. Additionally, cracks play a more significant role than solution cavities in affecting the wellbore stability. (3) When the orientation of a crack is closer to the direction of maximum horizontal stress, and the dip angle and width of the crack increase, the stress and deformation at the intersection of the crack and wellbore gradually increase, and correspondingly,  $\rho_c$  also increases. (4) The stress and displacement of various points around the solution cavities gradually increase with the increases in diameter and quantity of solution cavities, and  $\rho_c$  also increases. (5) Compared with the situation where cracks and solution cavities are not interconnected, the stress disturbance area around the wellbore is larger, and  $\rho_c$  is greater when cracks and solution cavities are interconnected.



**Citation:** Zhang, J.; Zhao, R.; An, H.; Li, W.; Geng, Y.; Fan, X.; Zhang, Q. Numerical Simulation on the Influence of the Distribution Characteristics of Cracks and Solution Cavities on the Wellbore Stability in Carbonate Formation. *Appl. Sci.* **2024**, *14*, 10099. <https://doi.org/10.3390/app142210099>

Academic Editor: Andrea Carpinteri

Received: 10 September 2024

Revised: 2 October 2024

Accepted: 2 October 2024

Published: 5 November 2024

**Keywords:** wellbore stability; dengying formation; carbonate rocks; cracks and solution cavities characteristics; numerical simulation



**Copyright:** © 2024 by the authors. Licensee MDPI, Basel, Switzerland. This article is an open access article distributed under the terms and conditions of the Creative Commons Attribution (CC BY) license (<https://creativecommons.org/licenses/by/4.0/>).

## 1. Introduction

Wellbore instability, which is the key to impeding quality and efficient drilling, is the focus of attention in the petroleum engineering field [1–6]. In particular, carbonate rocks are tricky for oil and gas drilling because they are full of unpredictable cracks and solution cavities [7–10]. These features can disrupt the pressure distribution and weaken the rock, leading to instability issues of the wellbore in the drilling process [11,12]. The instability of the wellbore in carbonate formation has perplexed engineers and researchers, even though this problem has been on the research radar for a while now [13–15], especially

since there is still a lot we do not know about how these cracks and solution cavities affect the wellbore stability.

It is a common understanding that cracks and solution cavities play a key role in affecting the wellbore stability in carbonate formation. Undoubtedly, the cracks can affect the rock's mechanical properties and fluid flow in the formation, resulting in instability of the wellbore. Yan et al. [16], Zhang et al. [17], Liu et al. [18], and Karatela et al. [19] pointed out that the crack's properties, such as strength and friction, are crucial for the wellbore stability. Cui et al. [20] discovered that the weak plane effect is significant, and the borehole wall is prone to collapse along the crack. Liu et al. [21] believe that the higher risk of wellbore instability may correspond to the formation with relatively high permeability, porosity, and gas saturation. Zhang et al. [22] found that cracks would promote rock hydration and then weaken the stability of the wellbore. On the other hand, the size and distribution of formation pores have a significant impact on wellbore stability. The size and distribution of pores can greatly affect the effectiveness of mud in supporting the wellbore [23]. Pore throats can affect the flow of drilling fluid in the formation and change the wellbore stability condition [24,25]. Moreover, pores can also impact the pore pressure distribution and ultimately result in a different wellbore collapse condition [26]. Researchers have tried various ways to evaluate the stability of wellbores in the formation of cracks and solution cavities. For example, Gentzis et al. [27] utilized lithological descriptions to predict rock strength parameters and subsequently introduced a wellbore stability evaluation method based on finite element theory. Based on a Monte Carlo probability analysis and the Mogi-Coulomb failure criterion, AI-Ajmi et al. [28,29] proposed a method for evaluating the wellbore collapse pressure of a carbonate reservoir. Karatela et al. [19] and Karatela and Taheri [30] established a discrete element numerical model to study the wellbore stability of fractured shale formation. Guo et al. [31] proposed a generalized H-B criterion model based on acoustic data for evaluating the wellbore stability of multi-set fractured limestone formation. Liu et al. [32] employed the fractal method to fit the functional relationship between the cohesion, internal friction angle, and fractal dimension of micro-fractured rocks and then developed a wellbore stability evaluation method for fractured carbonate formation. Based on the thermo-poroelastic medium theory, Gomar et al. [33] proposed a wellbore stability evaluation method for porous formation. These studies attempted to obtain a method to evaluate the wellbore stability of carbonate formation, considering the effect of cracks and solution cavities. Still, many of these studies did not fully address how unevenly distributed these cracks and solution cavities can be.

As mentioned above, although scholars have recognized that the development of cracks and solution cavities is a key factor influencing the wellbore stability of carbonate formation, and some methods for evaluating its wellbore stability were obtained, there is currently a lack of systematic research on the influence of the distribution characteristics of cracks and solution cavities on the wellbore stability in carbonate formation. In the present work, the characteristics of cracks and solution cavities, the mechanics properties of the carbonate rock in the Ordovician Dengying carbonate reservoir in the Gaoshiti–Moxi area of the Sichuan Basin are analyzed using log interpretation, electron microscope scanning experiments, and rock triaxial experiments. Then, employing the FLAC3D numerical simulation software, the influence of the distribution characteristics of cracks and solution cavities on the wellbore stability in carbonate formation is studied considering the orientation and dip angle of the crack, size, and quantity of solution cavities, connectivity of crack and solution cavity. These results can provide guidance for the drilling design in the carbonate formation with developed cracks and solution cavities.

## 2. Reservoir Rock Characteristics and Engineering Problems

### 2.1. Geological Features of the Dengying Formation Carbonate Reservoir

The Dengying Formation carbonate reservoir of the Gaoshiti–Moxi area in the Sichuan Basin sits within the Gaoshiti–Anpingdian–Moxi latent tectonic zone, depicted in Figure 1. This formation is located in the eastern part of the ancient Anyue–Suining–Tongnan up-

lift [34–36] and is characterized by its low and gentle structure. Shaped by intersecting structural lines running north to south and east to west, the area is marked by moderate elevations and a scarcity of faults. Notably, the seismic top structure here is more pronounced and enclosed than the cold top structure. The Dengying reservoir, known for its antiquity, exhibits notable plasticity and density, reinforced by strong compaction strength. Dominated by fractured-vuggy reservoirs, it is defined by its fragmented nature and limited capacity to withstand formation pressure. These geological features often lead to issues such as formation collapse, blockages, and stuck drill strings during drilling operations, presenting considerable challenges to the natural gas exploration and development efforts in the area.

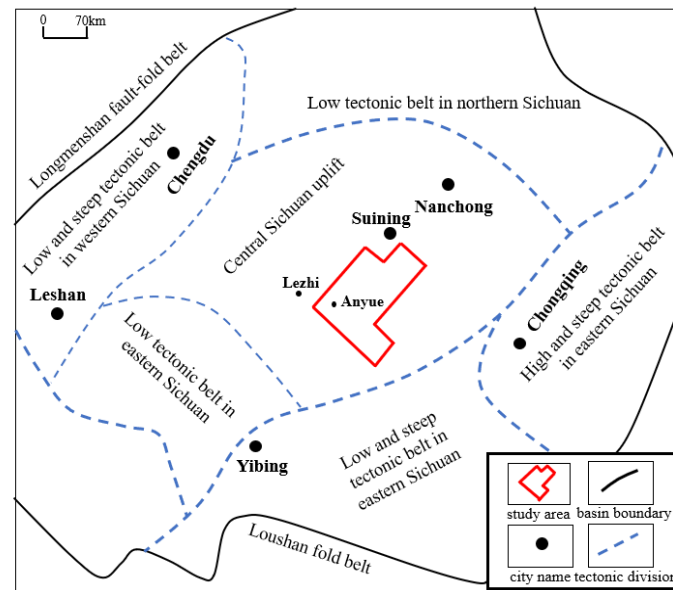


**Figure 1.** Reservoir geographical location and geological feature map.

## 2.2. Rock Cracks and Solution Cavities Characteristics

The rock samples were collected from the Dengying Formation at depths ranging from 4959 m to 5481 m of Well GS10 in the Gaoshiti–Moxi area of the Sichuan Basin using the core drill bit, as shown in Figure 2. These rock samples were obtained when the drilling operation reached the gas-producing reservoir. The dissolution pores in the rock of the Dengying Formation exhibit a variety of shapes, predominantly irregular or nearly circular. The distribution of these pores is notably uneven, often displaying band-like, honeycomb, patchy, and scattered arrangements. The formation is rich in solution cavities, with an average density of 26.45 per meter. Horizontal cracks are more common, followed by inclined ones. A large number of small cracks are also presented, with quantity densities ranging from 0.86 to 8.26 per meter. Notably, in the solution cavities and cracks, we observe fillings of quartz, dolomite, and asphalt. Additionally, some cracks are observed to be associated with solution cavities, indicating a complex interplay of geological processes.

## 2.3. Rock Mechanical Parameters

The triaxial compression tests on rock samples were conducted using a specialized apparatus (GCTS Ltd., RTR-1500, Tempe, AZ, USA), adhering to the method specified in the “Regulation for testing the physical and mechanical properties of rock—Part 20: Test for determining the strength of rock in triaxial compression” (Chinese Standard, Standard ID: DZ/T 0276.20-2015) [37]. The tests were carried out in accordance with the procedures detailed by Zhang et al. [38], using the samples extracted from the 5182 m to 5187 m depth interval of Well GS10, as shown in Figure 2. The results of these tests are listed in Table 1. A notable observation is the increase in rock compressive strength and elastic modulus with elevated confining pressure. However, the variation in the Poisson’s ratio with confining

pressure is not evident. A significant disparity in compressive strength is observed across different rock samples tested under identical confining pressure conditions. For instance, at a confining pressure of 50 MPa, the highest compressive strength recorded is 53.63% greater than the lowest. This substantial variation emphasizes the profound impact of cracks and solution cavities on the mechanical characteristics of carbonate rock, thus highlighting the distinct variability of the rock's mechanical parameters.



**Figure 2.** Rock samples collected from the Dengying Formation: (a) Brownish-gray solution cavities in dolomite at a depth from 5480.27 m to 5480.41 m; (b) Dark gray dolomite with solution cavities at a depth from 5460.12 m to 5460.22 m; (c) Light gray dolomite, at a depth from 4970.32 m to 4970.41 m; (d) Blackish-gray muddy dolomite, at a depth from 4959.81 m to 4959.89 m.

**Table 1.** Rock parameters of the carbonate rock tested by the triaxial compression tests.

No.	Compressive Strength/MPa	Elastic Modulus/GPa	Poisson's Ratio	Confining Pressure/MPa
1	143.61	33.45	0.23	0
2	264.20	46.32	0.32	50
3	415.38	53.55	0.24	60
4	174.99	41.10	0.22	0
5	402.31	48.84	0.29	50
6	390.08	50.06	0.26	60
7	197.03	36.20	0.23	0
8	358.30	49.30	0.27	50
9	383.27	50.01	0.23	60
10	253.11	38.41	0.24	0
11	261.86	49.34	0.21	50
12	391.34	49.19	0.28	60

#### 2.4. Wellbore Instability Problem

A critical wellbore collapse incident occurred at a depth ranging from 5182 m to 5187 m in Well GS10, which is located in the Gaoshiti–Moxi area of the Sichuan Basin. The target reservoir in this area is the Dengying Formation. The Dengying Formation was designed as the fifth opening section of Well GS10 with a drill bit diameter of 127 mm. This issue arose while using an oil-based drilling fluid with a density of 1.14 g/cm<sup>3</sup>, which was initially selected to prevent clay mineral hydration. However, this density decision did not factor in the presence of cracks and solution cavities, leading to mechanical instability. As a remedial measure, the density of the drilling fluid was increased to 1.24 g/cm<sup>3</sup>, which effectively resolved the issue, allowing for the successful completion of the drilling operation in this section. Subsequent imaging logging analysis highlighted the extensive development of cracks and solution cavities in the formation. As depicted in Figure 3, notable features included two large cracks with a dip angle of 19.81° and a maximum width of 10 mm and

three solution cavities, each with an average diameter of 10 mm. According to the cutting logging result based on the lithologic difference analysis, the maximum width of the crack is bigger than 30 mm, and the largest diameter of the solution cavity is approximately 900 mm. Therefore, the analysis concluded that these developed cracks and solution cavities were the key contributors to the wellbore instability due to the mechanical properties of the carbonate rocks decreasing significantly when the cracks and solution cavities appear in the rock. This indicates that the influence of the distribution characteristics of cracks and solution cavities on the wellbore stability in carbonate formation is worth further studying to optimize the drilling design on the new wells in this area.

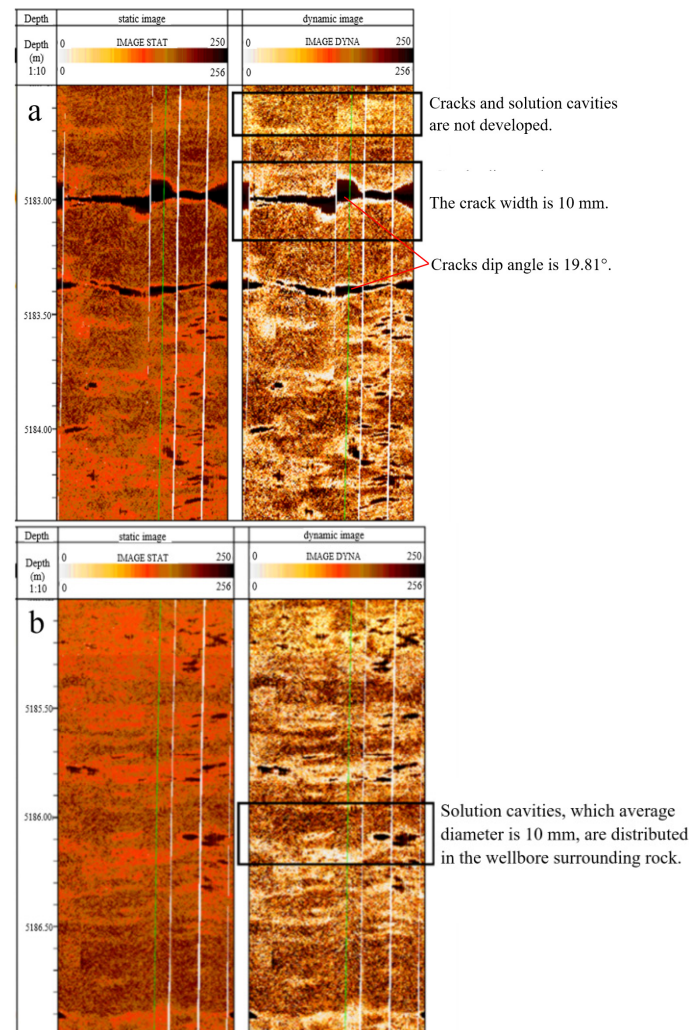


**Figure 3.** Distribution of cracks and solution cavities in the 5182–5187 m section of Well GS10 in the Gaoshiti–Moxi area of the Sichuan Basin: (a) 5182–5185 m section; (b) 5184.5–5187.5 m section.

### 3. Methodology and Model Parameters

#### 3.1. Numerical Simulation Scheme

According to the real-life scenario of cracks and solution cavities characteristics in the carbonate formation of the Gaoshiti–Moxi area of the Sichuan Basin (Figure 3), three factors are considered for evaluating the influence of cracks and solution cavities on the wellbore stability, including cracks characteristics, solution cavities characteristics and connectivity between cracks and solution cavities. Based on the formation reality stated in Section 3.1, the parameters setting of these factors in the numerical simulation is simplified through an arithmetic progression to obtain the favorable rules regarding the influence of cracks and solution cavities characteristics on the wellbore stability, as shown in Table 2. The

total stresses are employed to determine the stability of the wellbore. This is because the rock strength parameters, which are used for the numerical simulation, are calculated by using logging data. Additionally, there is another reason for using total stress. Considering the actual situation where a properly formed mud cake exists on the borehole wall, it is assumed that the gas in the formation does not flow. The equivalent drilling fluid density of collapse pressure ( $\rho_c$ ) is calculated for these different conditions to analyze these factors affecting the wellbore stability. The model designs of the angle of the crack strike and the maximum horizontal principal stress direction ( $\beta$ ), the dip angle of the crack ( $\theta$ ), the solution cavity diameter ( $D$ ), and the solution cavities quantity ( $N$ ) are shown in Figures 4–7, respectively.

**Table 2.** Parameters setting of the analytical factors for the numerical simulation.

Factor	Parameter	Parameters Setting	Other Parameters
Cracks characteristics	$\beta$	0°, 15°, 30°, 45°, 60°, 75°, 90°	$L_f = 10 \text{ mm}, \theta = 90^\circ$
	$\theta$	0°, 15°, 30°, 45°, 60°, 75°, 90°	$L_f = 10 \text{ mm}, \beta = 90^\circ$
	$L_f$	8 mm, 12 mm, 16 mm, 25 mm, 30 mm	$\beta = 90^\circ, \theta = 90^\circ$
Solution cavities characteristics	$D$	152 mm, 304 mm, 457 mm, 609 mm, 762 mm, 914 mm 1 (Unilateral distribution), 2 (Symmetrical distribution), 4 (Symmetrical distribution around the circumference), 8 (Symmetrical distribution around the circumference with two groups), 16 (Symmetrical distribution around the circumference with four groups)	$L = 300 \text{ mm}$
	$N$		$L = 300 \text{ mm}, D = 152 \text{ mm}$
Connectivity between cracks and solution cavities	Connectivity	Situation I: The cracks are not connected to the four solution cavities. Situation II: the cracks are connected to the four solution cavities.	$L_f = 10 \text{ mm}, D = 152 \text{ mm}$

$\beta$  is the angle of the crack strike and the maximum horizontal principal stress direction, °;  $\theta$  is the dip angle of the crack, °;  $L_f$  is the crack width, mm;  $D$  is the solution cavities diameter, mm;  $N$  is the solution cavities quantity, Integer;  $L$  is the distance from the solution cavities to the wellbore wall, mm.

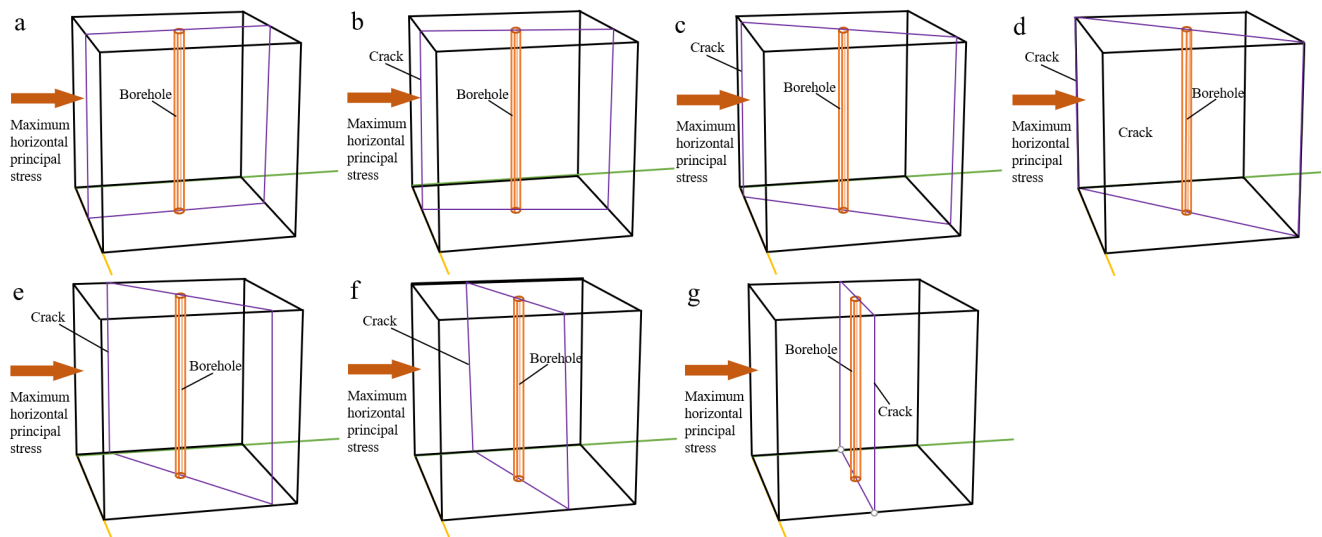


**Figure 4.** Model design of the angle of the crack strike and the maximum horizontal principal stress direction ( $\beta$ ): (a)  $\beta = 0^\circ$ ; (b)  $\beta = 15^\circ$ ; (c)  $\beta = 30^\circ$ ; (d)  $\beta = 45^\circ$ ; (e)  $\beta = 60^\circ$ ; (f)  $\beta = 75^\circ$ ; (g)  $\beta = 90^\circ$ .

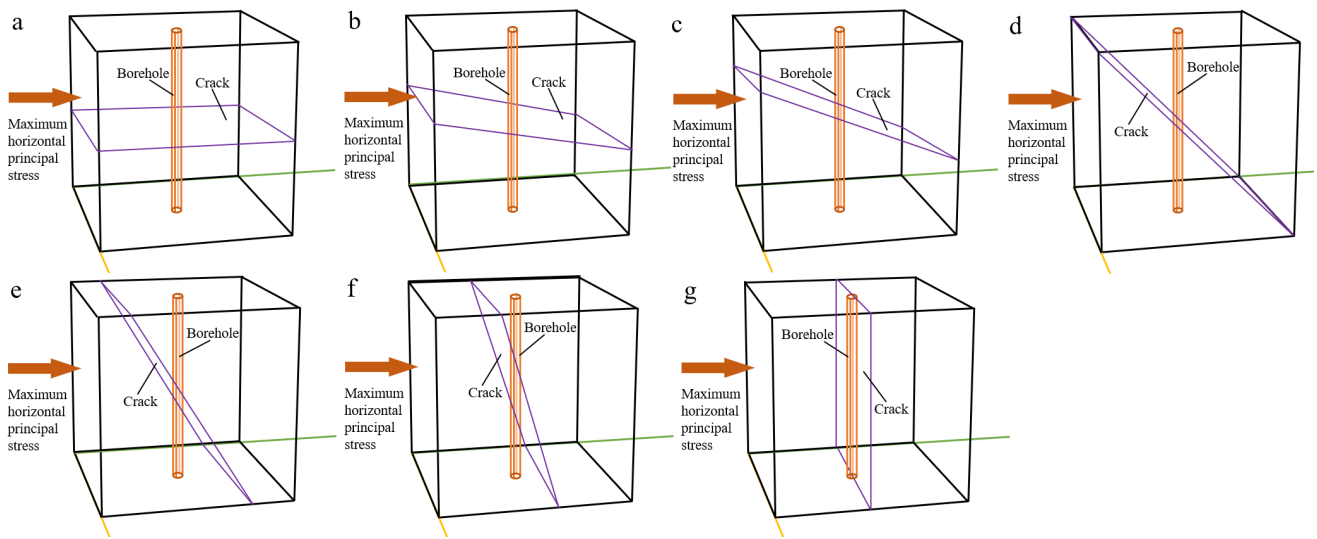


**Figure 5.** Model design of the dip angle of the crack ( $\theta$ ): (a)  $\theta = 0^\circ$ ; (b)  $\theta = 15^\circ$ ; (c)  $\theta = 30^\circ$ ; (d)  $\theta = 45^\circ$ ; (e)  $\theta = 60^\circ$ ; (f)  $\theta = 75^\circ$ ; (g)  $\theta = 90^\circ$ .

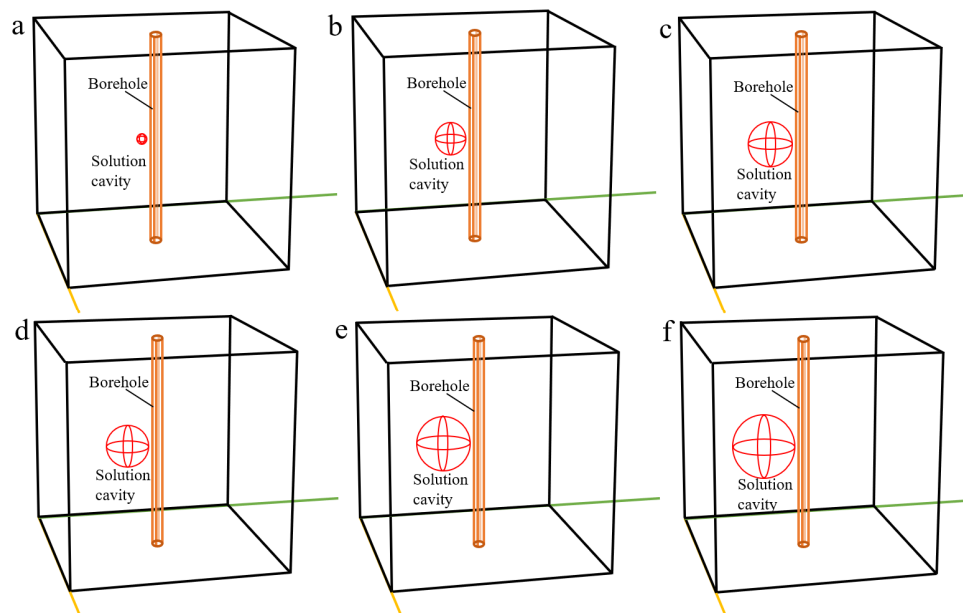


**Figure 6.** Model design of the solution cavity diameter ( $D$ ): (a)  $D = 152$  mm; (b)  $D = 304$  mm; (c)  $D = 457$  mm; (d)  $D = 609$  mm; (e)  $D = 762$  mm; (f)  $D = 914$  mm.

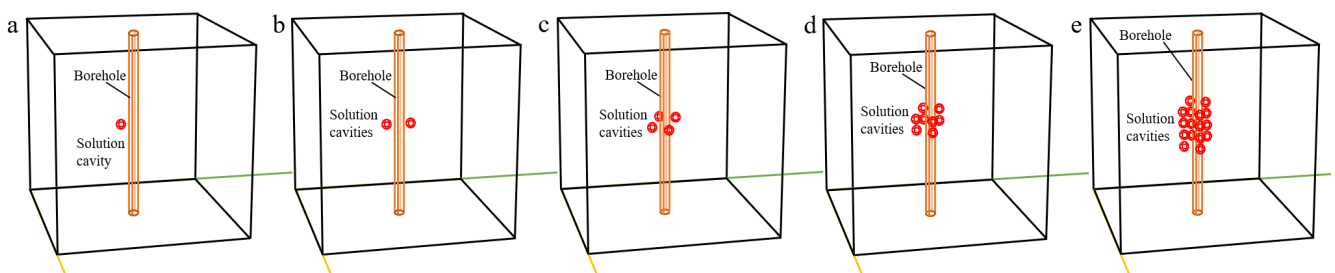


**Figure 7.** Model design of the solution cavities quantity ( $N$ ): (a)  $N = 1$ ; (b)  $N = 2$ ; (c)  $N = 4$ ; (d)  $N = 8$ ; (e)  $N = 16$ .

### 3.2. Numerical Simulation Method

The software FLAC3D, which is adept at calculating equivalent stress by assessing the equivalent plastic strain, was employed for the numerical simulations. It is vital to determine the stress state after the plastic yield of the surrounding rock. When the wellbore rock's plastic yield value surpasses its critical threshold, the convergence of the calculation should be judged. If the calculation cannot converge, it signals a state of instability and the potential failure of the surrounding rock.

Following the factors and parameters detailed in Table 2, the numerical simulation to assess the influence of cracks and solution cavities on wellbore stability comprises several stages:

- (1) The stratum model containing the cracks and solution cavities according to the parameters setting as shown in Table 2 is created, the model parameters are set, and initial stress and pore pressure are applied to the model. The model then undergoes a calculation phase to achieve stress balance.
- (2) Within this stratum model, a borehole is simulated. Since the main concern is the deformation of the strata around the wellbore, the inside of the wellbore is set as a certain pressure boundary condition considering the supporting effect of drilling fluid on the wellbore wall. To ensure the stability of the rock surrounding the wellbore, a high fluid column pressure is applied in the borehole at first.
- (3) The fluid column pressure is gradually decreased. The point at which the wellbore collapses with a fluid column pressure ( $P_c$ ) is determined by the onset of plastic deformation without a convergence result in the surrounding rock, and the Mohr–Coulomb criterion is used to justify this plastic deformation. From this, the equivalent drilling fluid density of collapse pressure ( $\rho_c$ ) is calculated by dividing  $P_c$  by the formation depth ( $H$ ).

The numerical simulation flow chart is illustrated in Figure 8.

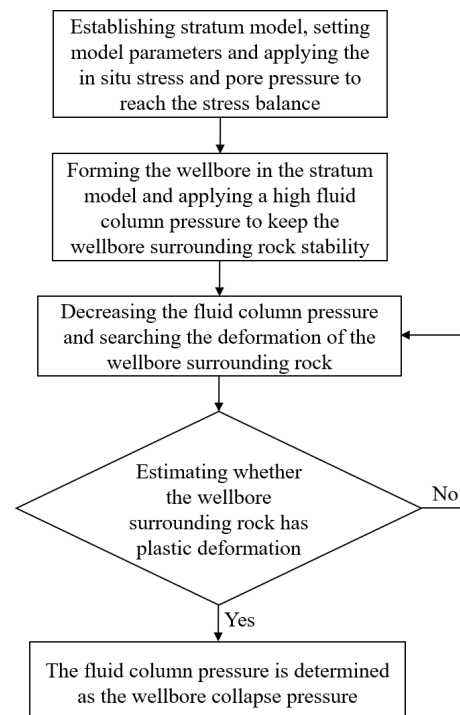


**Figure 8.** Numerical simulation flow chart.

### 3.3. Numerical Simulation Model

The numerical simulation model is designed as a 3-m cube featuring a vertical wellbore at its center to replicate an actual wellbore, as illustrated in Figure 9a. In this setup, the four

lateral sides of the model are fixed horizontally, while vertically, they are subject to free boundary conditions. Normal stress is applied to the model's outer boundaries to maintain a balance between the internal and external forces. Given that the stresses in all three directions exceed 120 MPa, the gravitational effect on the cube is considered negligible. The mesh layout of the model is displayed in Figure 9b. A more accurate simulation result can be obtained when a denser mesh is set compared to when a sparse mesh is set for numerical simulation; thus, a denser mesh is generated around the wellbore area. After establishing the numerical simulation model, as shown in Figure 9, the rock, cracks, and solution cavities are generated by changing the material parameters of the designated area in the numerical simulation model according to the numerical simulation scheme, as introduced in Section 3.1.

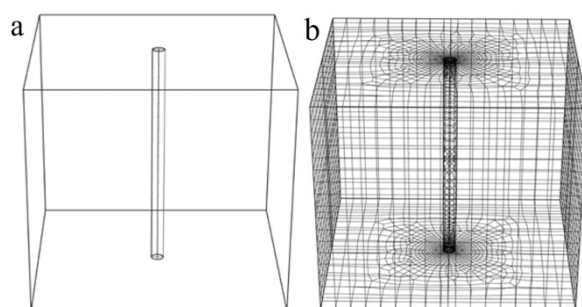


**Figure 9.** Numerical simulation model (a) and mesh generation (b).

#### 3.4. Model Parameters

By utilizing the well logging data for the 5182 m–5187 m section of Well GS10 (as shown in Figure 10), the pore pressure and three in situ stresses (overburden pressure, minimum principal stress, and maximum principal stress) were determined. The pore pressure was calculated using the Eaton method [39], and the three in situ stresses were calculated using Huang's model [40]. The parameters of the numerical simulation are presented in Table 3. Due to the discrepancy in stress conditions between rock core tests and the actual formation, rock parameters were first calculated using logging data and then corrected with test results. Therefore, the rock strength parameters in Table 3 are determined by total stresses since effective stress cannot be determined through well logging interpretation.

**Table 3.** Parameters for numerical simulation.

Parameter	Value
Maximum horizontal stress/MPa	154.08
Minimum horizontal stress/MPa	122.49
Vertical stress/MPa	142.58
Formation pressure/MPa	65.00
Elastic modulus of rock/GPa	49.52
Poisson's ratio of rock	0.28
Cohesion of rock/MPa	20.52
Internal friction angle of rock/°	39.60
Elastic modulus of the fillings in cracks/GPa	25.68
Poisson's ratio of the fillings in cracks	0.23
Cohesion of the fillings in cracks/MPa	7
Internal friction angle of the fillings in cracks/°	25.90
Elastic modulus of the fillings in solution cavities/GPa	3.85
Poisson's ratio of the fillings in solution cavities	0.13
Cohesion of the fillings in solution cavities/MPa	7
Internal friction angle of the fillings in solution cavities/°	3.20

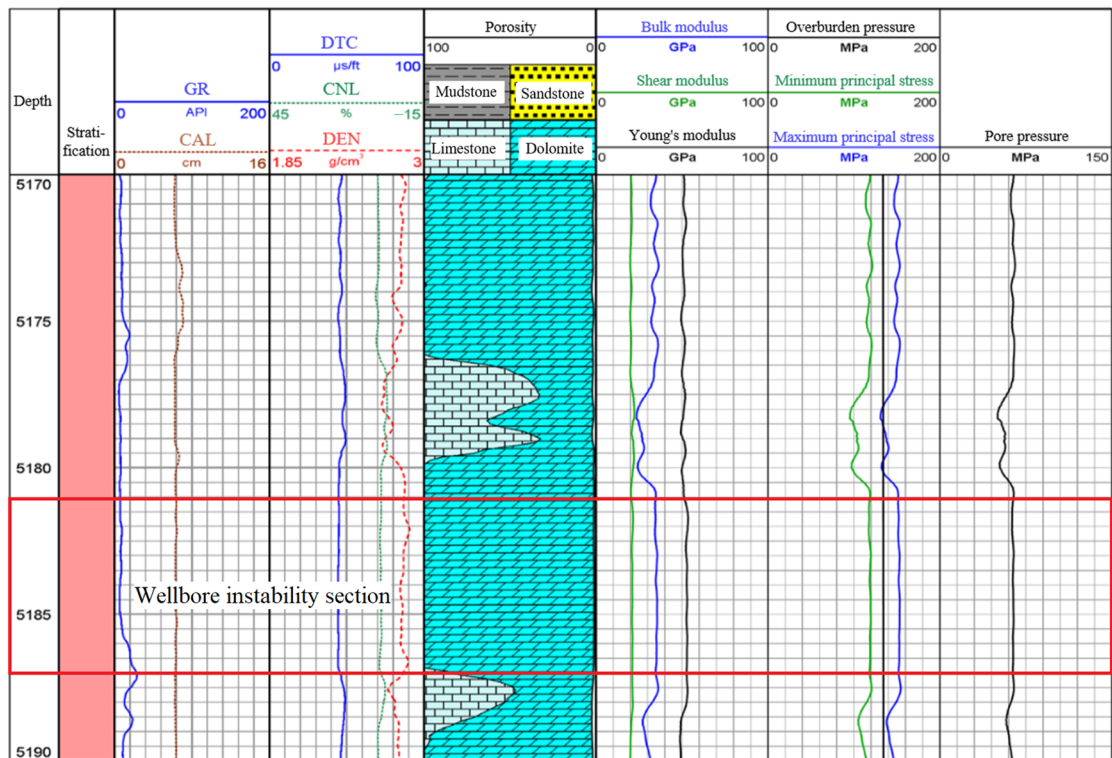


**Figure 10.** Geomechanical parameters of the 5170–5190 m section of Well GS10 obtained from well logging interpretation.

#### 4. Results and Analysis

##### 4.1. Verification of the Numerical Simulation Results

Reflecting the imaging log data for the 5182–5187 m section of Well GS10, the numerical model was designed to explore three situations: one without the influence of cracks and solution cavities, another considering only the presence of cracks, and the third one encompassing both cracks and solution cavities. In the latter two situations, the cracks and solution cavities were determined based on the imaging logging chart, as depicted in Figure 3. Two cracks with a dip angle of 19.81° were designed to cross the well in the model. The width of one crack was 10 mm, while the width of the other was 3 mm. Ten solution cavities were designed around the well, with diameters ranging from 3 mm to 20 mm and an average value of 10 mm. The third case was consistent with the actual situation on the site. Following the methodology mentioned in Section 3, the equivalent drilling fluid densities of collapse pressure ( $\rho_c$ ) were calculated for these varied conditions, as shown in Table 4. Notably,  $\rho_c$  considering the impacts of both cracks and solution cavities increases by 6.42% compared to ignoring cracks and solution cavities. Furthermore,  $\rho_c$  considering both cracks and solution cavities increases by 1.75% compared with the value for only considering cracks, and  $\rho_c$  considering only cracks increases by 4.59% compared with the value for ignoring cracks and solution cavities. This indicates that cracks play a more significant role than solution cavities in affecting the wellbore stability.

From a practical standpoint, as discussed in Section 3.1, the initial employment of an oil-based drilling fluid with a density of 1.14 g/cm<sup>3</sup>, which overlooked the effects of cracks and solution cavities, resulted in significant wellbore collapse. Adjusting the drilling fluid density to 1.24 g/cm<sup>3</sup> subsequently alleviated this problem. This practical situation corresponds well with our simulation findings in Table 4, reinforcing the validity of our numerical approach. By accounting for both cracks and solution cavities, this method offers a more accurate and dependable means for assessing wellbore stability in the Dengying Formation carbonate reservoir in the Gaoshiti–Moxi area of the Sichuan Basin.

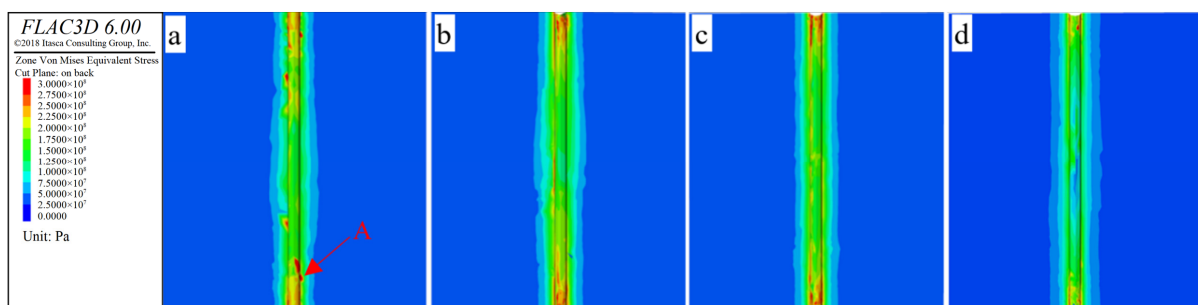
**Table 4.** Equivalent drilling fluid densities of collapse pressure for the three situations.

Situation	Description	Result/g·cm <sup>-3</sup>
Without considering cracks and solution cavities	The formation is considered as the intact rock	1.09
Only considering cracks	Two cracks with a dip angle of 19.81° are designed in the formation model. The width of one crack is 10 mm, while the width of the other is 3 mm	1.14
Considering cracks and solution cavities	Two cracks with a dip angle of 19.81° and ten solution cavities are designed in the formation model. The width of one crack is 10 mm, while the width of the other is 3 mm. The diameters of the solution cavities range from 3 mm to 20 mm, with an average value of 10 mm. This situation is consistent with the actual situation on the site	1.16

#### 4.2. Influence of Cracks Characteristics on the Wellbore Stability

##### 4.2.1. Influence of Crack Orientation on the Wellbore Stability

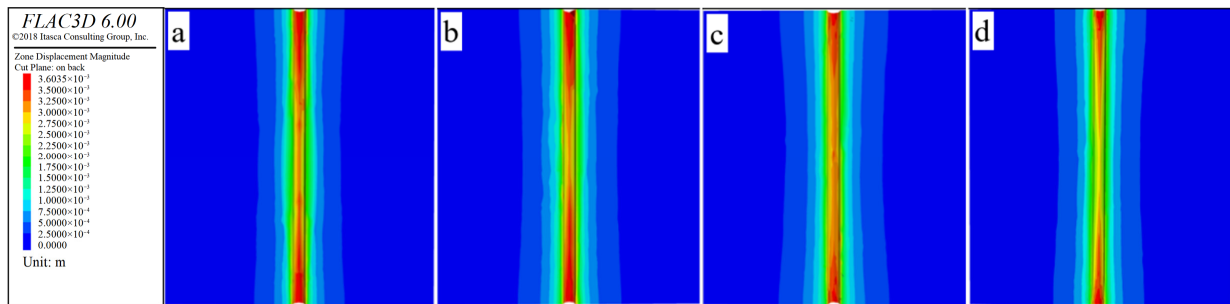
Figures 11 and 12 present the stress and displacement patterns around the wellbore, varying with the angle ( $\beta$ ) between the crack strike and the maximum horizontal principal stress direction, as shown in Table 2. The observed trend is the following: with a decrease in  $\beta$ , both the stress and displacement at all points around the wellbore gradually increase. The lowest stress and displacement values are recorded when  $\beta$  equals 90°. For instance, at  $\beta = 0^\circ$ , the stress and displacement at point A are measured at 125.21 MPa and 1.53 mm, respectively. In contrast, at  $\beta = 90^\circ$ , these values drop to 105.61 MPa and 1.25 mm, representing decreases of 15.65% and 18.30%, respectively. This pattern suggests that when cracks align parallel to the maximum horizontal principal stress, the stress and deformation at the crack-wellbore intersection are at their peak. Conversely, these values progressively reduce as  $\beta$  increases. This can be attributed to the following reasons: At  $\beta = 0^\circ$ , the maximum horizontal stress causes the cracks near the wellbore to undergo tensile expansion, leading to concentrated stress and increased tensile displacement in the area. However, at  $\beta = 90^\circ$ , the maximum horizontal stress tends to close the cracks, resulting in lesser stress concentration and tensile displacement compared to the former situation.



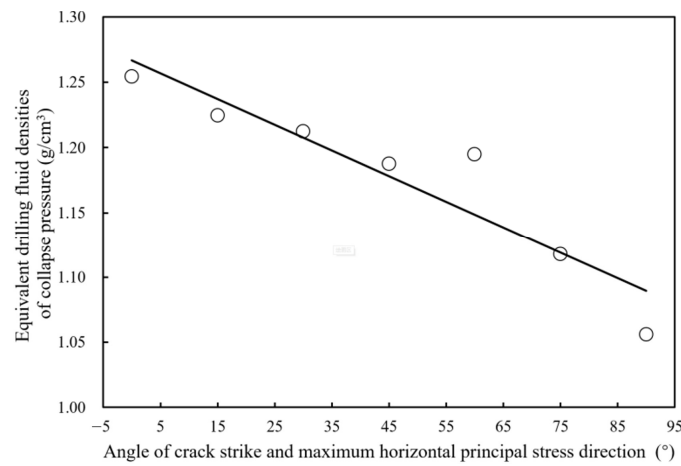
**Figure 11.** Stress nephogram around the wellbore at different  $\beta$ : (a)  $\beta = 0^\circ$ ; (b)  $\beta = 30^\circ$ ; (c)  $\beta = 60^\circ$ ; (d)  $\beta = 90^\circ$ .

Figure 13 showcases the correlation between the equivalent drilling fluid densities of collapse pressure ( $\rho_c$ ) and the angle ( $\beta$ ) between the crack strike and the maximum horizontal principal stress direction. A notable trend emerges from the graph:  $\rho_c$  linearly diminishes with an increase in  $\beta$ . Specifically,  $\rho_c$  is 1.26 g/cm<sup>3</sup> at  $\beta = 0^\circ$  but drops to 1.06 g/cm<sup>3</sup> at  $\beta = 90^\circ$ , marking a substantial reduction of 15.87%. When considered alongside the previously discussed stress and displacement data, this trend suggests a clear rule: in situations where cracks run parallel to the maximum horizontal stress, vertical cracks intersecting the wellbore are prone to tensile expansion. This expansion significantly

contributes to the weakening and potential failure of the rock formation surrounding the wellbore, thus resulting in the highest collapse pressure under these conditions.



**Figure 12.** Displacement nephogram around the wellbore at different  $\beta$ : (a)  $\beta = 0^\circ$ ; (b)  $\beta = 30^\circ$ ; (c)  $\beta = 60^\circ$ ; (d)  $\beta = 90^\circ$ .



**Figure 13.** Curve between the equivalent drilling fluid density of collapse pressure and the angle of the crack strike and maximum horizontal principal stress direction.

#### 4.2.2. Influence of Crack Dip Angle on the Wellbore Stability

Figures 14 and 15 illustrate the variations in stress and displacement around the wellbore in response to different crack dip angles ( $\theta$ ). Analyzing these figures leads to two significant observations: First, an increase in  $\theta$  results in both stress and displacement at points around the wellbore. For example, at  $\theta = 0^\circ$ , the stress and displacement at point A are recorded at 82.58 MPa and 0.85 mm, respectively. At a higher angle of  $\theta = 60^\circ$ , these values increase to 102.56 MPa and 1.08 mm, indicating increases of 24.08% and 27.05%, respectively. The rationale behind this trend is that as  $\theta$  increases, more points along the crack surface come closer to the wellbore. This proximity weakens the integrity of the surrounding rock layers, preventing the formation of a uniformly stressed, arch-like structure around the wellbore. Consequently, areas where cracks intersect the wellbore experience heightened stress concentration and larger displacement, as shown in Figures 14 and 15.

Figure 16 presents the relationship between the equivalent drilling fluid density of collapse pressure ( $\rho_c$ ) and the crack dip angle ( $\theta$ ). The graph in Figure 16 illustrates that  $\rho_c$  exhibits a linear increase as  $\theta$  rises. For instance,  $\rho_c$  is calculated at 1.08 g/cm<sup>3</sup> at  $\theta = 0^\circ$ , and it escalates to 1.41 g/cm<sup>3</sup> at  $\theta = 90^\circ$ , representing a substantial increase of 30.56% from the initial value. Correlating this with the stress and displacement changes depicted in Figures 14 and 15, it becomes evident that an increase in  $\theta$  adversely affects the integrity of the rock surrounding the wellbore. This weakening of the rock structure makes the wellbore more prone to damage, thus leading to an increase in  $\rho_c$  with the rising  $\theta$ .

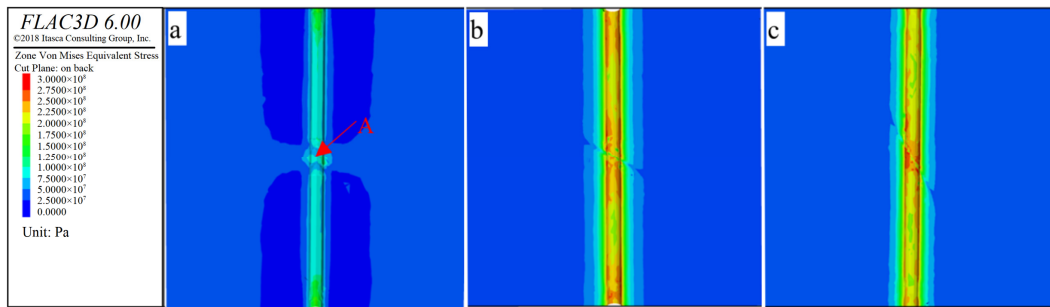


**Figure 14.** Stress nephogram around the wellbore for different crack dip angles: (a)  $\theta = 0^\circ$ ; (b)  $\theta = 30^\circ$ ; (c)  $\theta = 60^\circ$ .

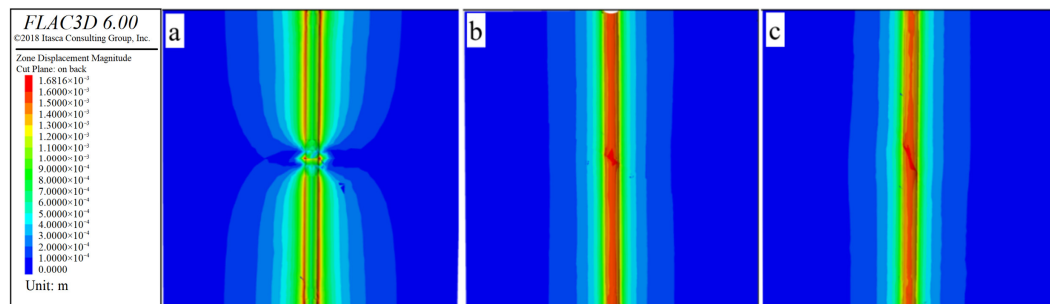


**Figure 15.** Displacement nephogram around the wellbore for different crack dip angles: (a)  $\theta = 0^\circ$ ; (b)  $\theta = 30^\circ$ ; (c)  $\theta = 60^\circ$ .

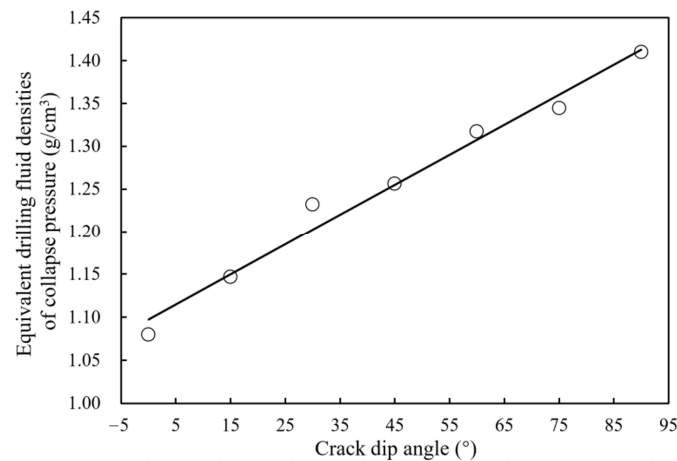


**Figure 16.** Curve between the equivalent drilling fluid densities of collapse pressure and crack dip angles.

#### 4.2.3. Influence of Crack Width on the Wellbore Stability

Figures 17 and 18 illustrate the variations in stress and displacement around the wellbore concerning various crack widths ( $L_f$ ). Notably, both the stress and the displacement at different locations around the wellbore increase gradually as  $L_f$  increases. For example, when  $L_f$  is 8 mm, the stress and displacement values at point A are 108.23 MPa and 1.27 mm, respectively. However, when  $L_f$  is 30 mm, the stress and displacement values at point A rise to 146.32 MPa and 1.52 mm, respectively. This represents a substantial increase of 35.13% in stress and 19.68% in displacement compared to the previous values. This trend underscores the fact that an expansion in the crack width leads to a reduction in the stability of the surrounding rock, consequently resulting in elevated stress and displacement levels at various points around the wellbore.

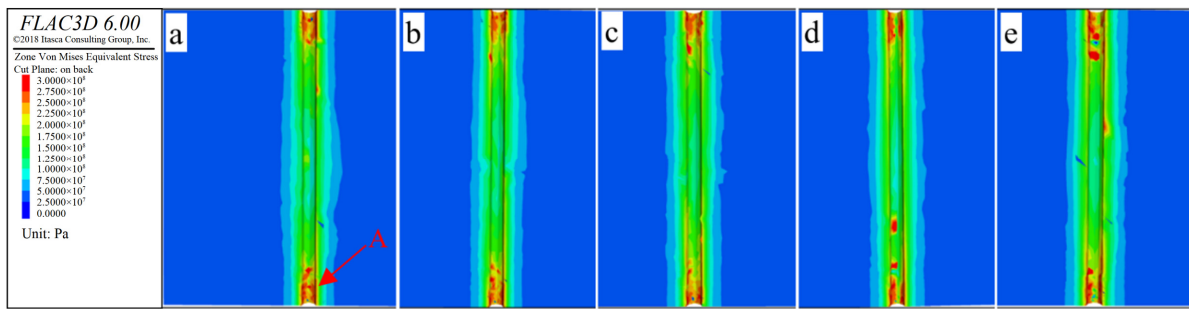


**Figure 17.** Stress nephogram around the wellbore for different crack widths: (a)  $L_f = 8$  mm; (b)  $L_f = 12$  mm; (c)  $L_f = 16$  mm; (d)  $L_f = 25$  mm; (e)  $L_f = 30$  mm.

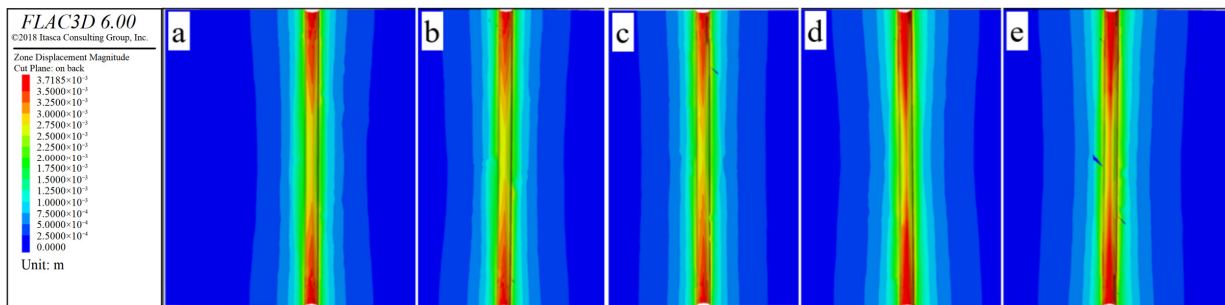


**Figure 18.** Displacement nephogram around the wellbore for different crack widths: (a)  $L_f = 8$  mm; (b)  $L_f = 12$  mm; (c)  $L_f = 16$  mm; (d)  $L_f = 25$  mm; (e)  $L_f = 30$  mm.

Figure 19 presents the relationship between the equivalent drilling fluid densities of collapse pressure ( $\rho_c$ ) and crack widths ( $L_f$ ). It is evident from the figure that  $\rho_c$  exhibits a linear increase with the increase in  $L_f$ . For example, when  $L_f$  is 8 mm,  $\rho_c$  is measured as 1.06 g/cm<sup>3</sup>, while for  $L_f = 30$  mm,  $\rho_c$  increases to 1.33 g/cm<sup>3</sup>, representing a 25.47% increment compared to the previous value. This observed increase can be attributed to the reduced stability of the rock surrounding the wellbore as  $L_f$  increases, resulting from stress concentration near the cracks, as demonstrated in Figure 17. Consequently,  $\rho_c$  exhibits an upward trend with the growth of  $L_f$ .

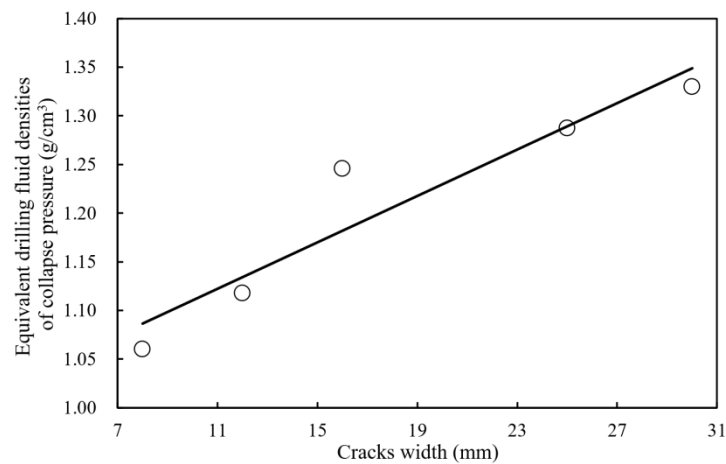


**Figure 19.** Curve between the equivalent drilling fluid densities of collapse pressure and crack widths.

### 4.3. Influence of Solution Cavities Characteristics on the Wellbore Stability

#### 4.3.1. Influence of Solution Cavities Size on the Wellbore Stability

Figures 20 and 21 present the variations in stress and displacement around the wellbore for various solution cavity diameters ( $D$ ). These figures reveal a consistent trend: stress and displacement at different locations around the wellbore gradually increase with an increase in  $D$ . For instance, when  $D$  is 152 mm, the stress and displacement values at point A are measured as 201.03 MPa and 3.52 mm, respectively. However, with  $D$  increased to 914 mm, the stress and displacement at point A rise to 256.32 MPa and 4.03 mm, respectively. This represents a significant increase of 28.01% in stress and 14.48% in displacement compared to the previous values.

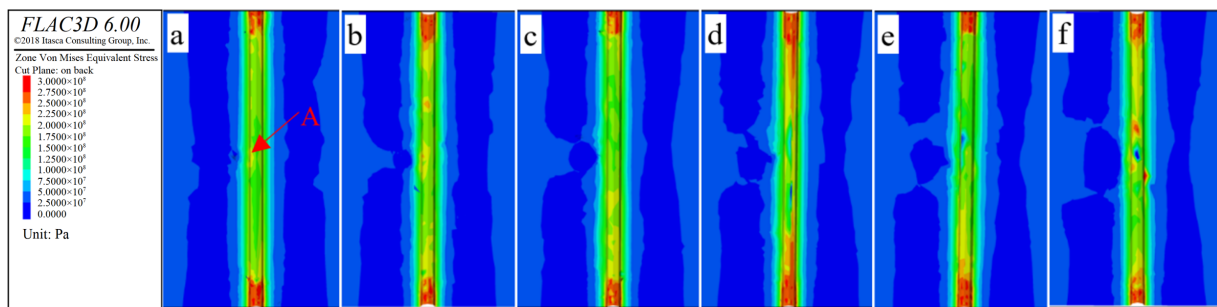


**Figure 20.** Stress nephogram around the wellbore for different solution cavities diameter: (a)  $D = 152$  mm; (b)  $D = 304$  mm; (c)  $D = 457$  mm; (d)  $D = 609$  mm; (e)  $D = 762$  mm; (f)  $D = 914$  mm.

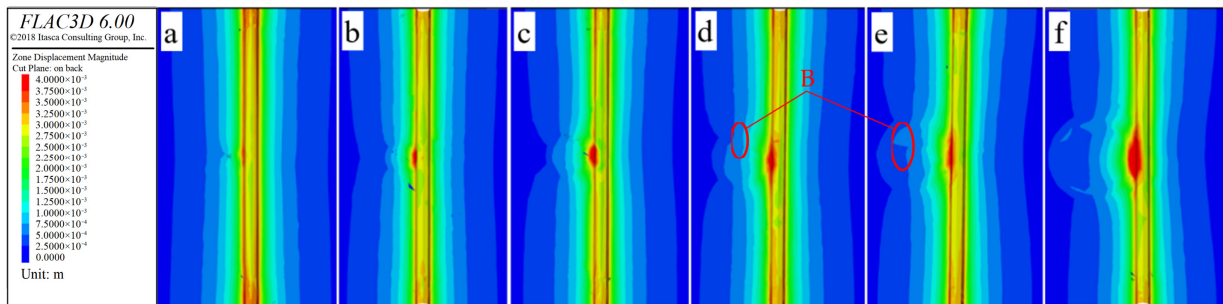


**Figure 21.** Displacement nephogram around the wellbore for different solution cavities diameter: (a)  $D = 152$  mm; (b)  $D = 304$  mm; (c)  $D = 457$  mm; (d)  $D = 609$  mm; (e)  $D = 762$  mm; (f)  $D = 914$  mm.

This phenomenon can be attributed to the lower mechanical strength of the fillings within the solution cavities compared to the surrounding rock. In such cases, stress tends to concentrate on the solution cavities wall due to the limited supporting capacity of the fillings, as exemplified by the conditions observed at point A in Figure 20. Furthermore, this stress concentration amplifies with the enlargement of  $D$ , leading to increased deformation in the solution cavities area, as shown in Figure 21.

Figure 22 presents the relationship between the equivalent drilling fluid densities of collapse pressure ( $\rho_c$ ) and solution cavities diameter ( $D$ ). The figure reveals an initial linear increase in  $\rho_c$  with the growth of  $D$ , and  $\rho_c$  for the situation of  $D = 609$  mm is increased by 14.12% compared with the situation of  $D = 152$  mm. However, when  $D$  exceeds 609 mm, there is no significant change in  $\rho_c$ . This phenomenon can be ascribed to the fact that when the size of the solution cavities reaches a certain value, for example,  $D = 609$  mm, it may cause wellbore collapse and damage to the surrounding rock mass, thereby forming a substantial cavity. As shown in Figure 21, the area (area B) with a displacement larger than 3.5 mm for  $D = 609$  mm increases sharply compared to that for  $D = 457$  mm. In this case, the main factor affecting wellbore stability would be the damage to the rock between the solution cavity and the borehole, and this cavity may become large enough to minimize the

impact of further increases in solution cavity size on  $\rho_c$ . Therefore, the linear relationship between the diameter of solution cavities and  $\rho_c$  rises to 609 mm and then becomes flat.

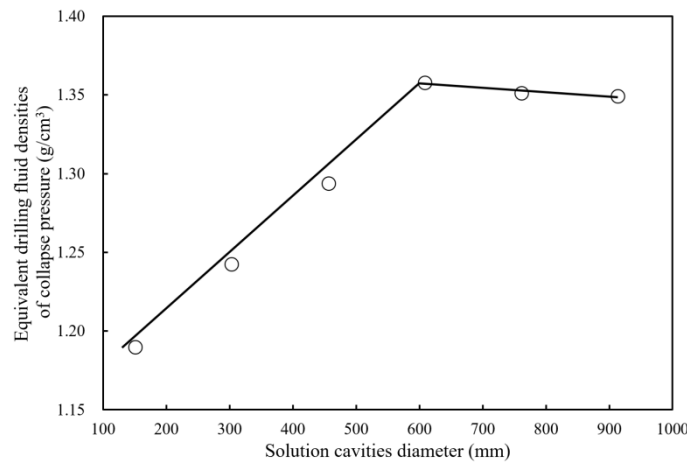


**Figure 22.** Curve between the equivalent drilling fluid densities of collapse pressure and solution cavities diameter.

#### 4.3.2. Influence of Solution Cavities Quantity on Wellbore Stability

Figures 23 and 24 illustrate the variations in stress and displacement distribution around the wellbore for varying solution cavity quantities ( $N$ ). Notably, these figures illustrate a consistent trend: as solution cavities quantity ( $N$ ) increases, both stress and displacement around the wellbore gradually rise. For example, when  $N = 1$ , the stress and displacement values at point A are measured as 165.42 MPa and 2.78 mm, respectively. However, with an increase in  $N$  to 16, the stress and displacement at point A increase to 178.62 MPa and 2.92 mm, respectively. This marks a notable increase of 7.98% in stress and 5.03% in displacement compared to the previous values.

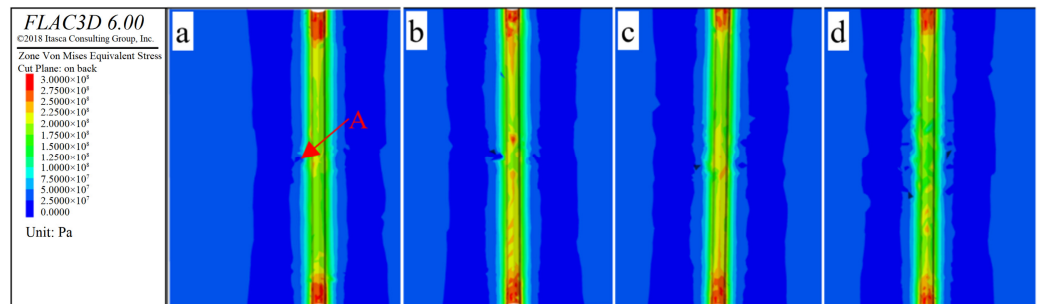


**Figure 23.** Stress nephogram around the wellbore for different solution cavities quantities: (a)  $N = 1$ ; (b)  $N = 4$ ; (c)  $N = 8$ ; (d)  $N = 16$ .

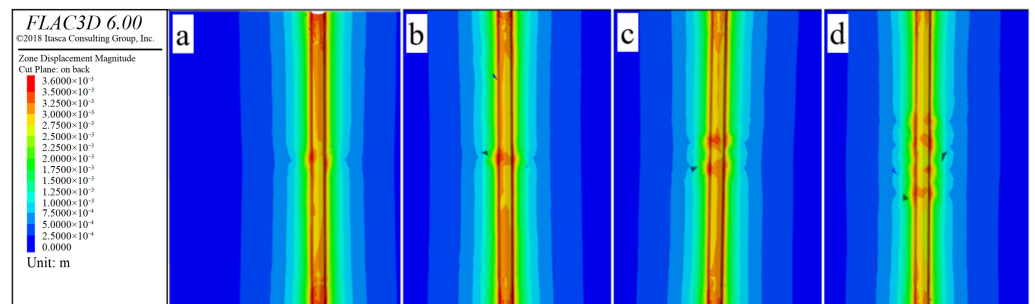


**Figure 24.** Displacement nephogram around the wellbore for different solution cavities quantities: (a)  $N = 1$ ; (b)  $N = 4$ ; (c)  $N = 8$ ; (d)  $N = 16$ .

This trend can be attributed to the fact that an increase in the quantity of solution cavities near the wellbore can compromise the integrity of the rock, significantly reducing the stability of the surrounding rock mass. Consequently, stress and displacement around the wellbore, particularly in proximity to the solution cavities, increase as  $N$  grows.

Figure 25 presents the relationship between the equivalent drilling fluid densities of collapse pressure ( $\rho_c$ ) and the number of solution cavities ( $N$ ). Figure 25 reveals an approximately linear increase in  $\rho_c$  with the growth of  $N$ . For instance, when  $N = 1$ ,  $\rho_c$  is measured at  $1.18 \text{ g/cm}^3$ , whereas for  $N = 16$ ,  $\rho_c$  increases to  $1.31 \text{ g/cm}^3$ . This represents a notable increase of 11.02% compared to the previous value. This trend indicates that wellbore stability would significantly decrease with an increase in the number of solution cavities. This decrease in stability is attributed to the compromised integrity of the rock surrounding the wellbore, as mentioned above.

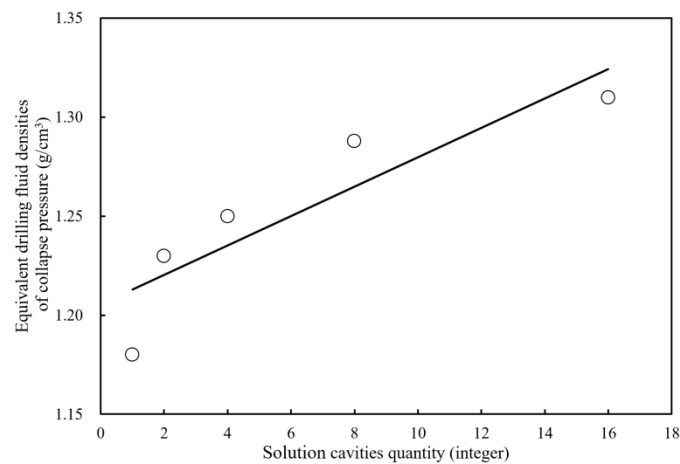


**Figure 25.** Curve between the equivalent drilling fluid densities of collapse pressure and solution cavities quantities.

#### 4.4. Influence of Connectivity Between Cracks and Solution Cavities on the Wellbore Stability

Figures 26 and 27 illustrate the variations in stress and displacement distribution around the wellbore under different conditions of cracks and solution cavities connectivity. Figure 22 shows the following: (1) The disturbed stress area around the wellbore is 45.23% larger for the condition of connected cracks and solution cavities compared to the condition of disconnected cracks and solution cavities. (2) The stress around the wellbore is higher when the cracks and solution cavities are connected. For instance, when the cracks and solution cavities are disconnected, the stress at point A is measured as 222.25 MPa. However, when the cracks and solution cavities are connected, the stress at point A increases to 278.62 MPa, representing a 25.36% increase compared to the previous condition. As for Figure 27, it is observed that the connectivity of cracks and solution cavities has an insignificant impact on the displacement of various points around the wellbore. This may be because the connectivity of cracks and solution cavities does not significantly affect the integrity of the surrounding rock, resulting in minimal differences in rock deformation around the wellbore. However, when cracks extend through the solution cavities into the formation, deformation of the solution cavities might lead to stress release, which would increase the influence of cracks on the stress distribution around the wellbore. Consequently, stress disturbance for the condition of connected cracks and solution cavities would expand compared to the condition of disconnected cracks and solution cavities.

The equivalent drilling fluid densities of collapse pressure ( $\rho_c$ ) under the conditions of disconnected and connected cracks and solution cavities are  $1.202 \text{ g/cm}^3$  and  $1.362 \text{ g/cm}^3$ , respectively. It reveals that  $\rho_c$  for the condition of connected cracks and solution cavities increases by 13.33% compared to that for the condition of disconnected cracks and solution cavities. This emphasizes the importance of carefully surveying the connectivity of cracks

and solution cavities during drilling design. It also highlights the need to pay greater attention to carbonate formation with connected cracks and solution cavities during the drilling process in such formation.

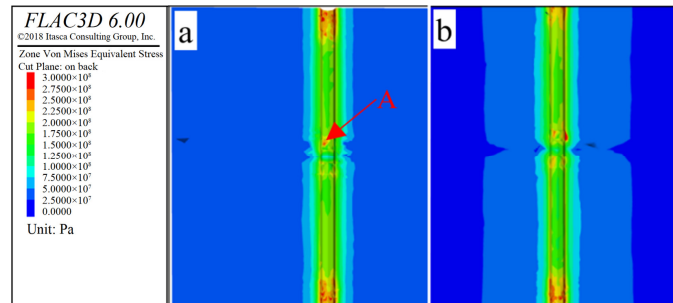


**Figure 26.** Stress nephogram around the wellbore for (a) disconnected cracks and solution cavities; (b) connected cracks and solution cavities.

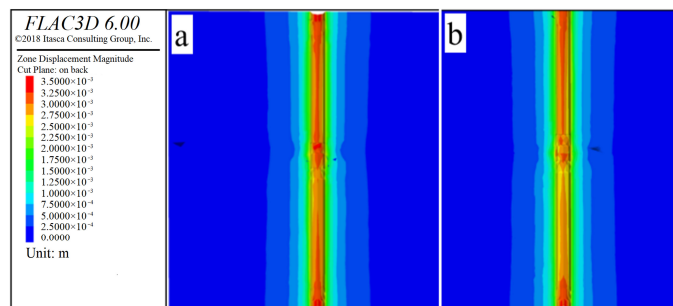


**Figure 27.** Displacement nephogram around the wellbore for (a) disconnected cracks and solution cavities; (b) connected cracks and solution cavities.

#### 4.5. Sensitivity Analysis of Cracks and Solution Cavities Characteristics on the Wellbore Stability

Figure 28 shows the percentage of the maximum change in the equivalent densities of collapse pressure under the circumstances of variations in crack orientation, crack dip angle, crack width, solution cavities size, solution cavities quantity, and the connectivity between cracks and solution cavities. As shown in Figure 28, cracks have a much more significant impact on wellbore stability than solution cavities. When comparing the influencing factors such as the orientation, dip angle, and width of cracks, the wellbore stability is most sensitive to the crack dip angle, followed by the crack width and crack orientation. For example, the equivalent drilling fluid densities of collapse pressure ( $\rho_c$ ) for a crack dip angle ( $\theta$ ) of  $90^\circ$  is 30.55% higher than that for  $\theta = 0^\circ$ ;  $\rho_c$  for a crack width ( $L_f$ ) of 8 mm is 25.47% higher than that for  $L_f = 30$  mm; and  $\rho_c$  for a crack orientation ( $\beta$ ) of  $0^\circ$  is 15.87% higher than that for  $\beta = 90^\circ$ . Regarding the influencing factor of the solution cavity characteristics, the solution cavity size has the greatest impact on the wellbore stability, followed by the connectivity between cracks and solution cavities and the solution cavities quantity. However, the difference in the influence among these solution cavities characteristics factors is smaller than that of the cracks characteristics factors. It should be noted that the sensitivity analysis of cracks and solution cavities characteristics on wellbore stability here is based on the numerical simulation conditions and parameter settings, as shown in Section 3.2, which is in line with the real-life scenario of cracks and solution cavities characteristics in the carbonate formation in the Gaoshiti–Moxi area of the Sichuan Basin. The results of the sensitivity analysis may be different if other formations or geological conditions are studied.

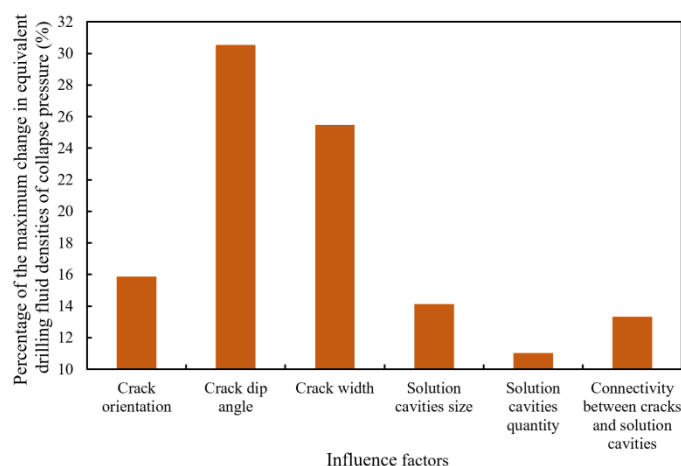


**Figure 28.** Percentage of the maximum change in the equivalent drilling fluid densities of collapse pressure for different influence factors.

As previously discussed, the presence of cracks and solution cavities in carbonate formation significantly diminishes the wellbore stability. In the case of vertical wells, cracks oriented closer to the direction of maximum horizontal stress can lead to reduced wellbore stability. Furthermore, the increased dip angle and width of cracks, along with the greater quantity and size of solution cavities, including connected cracks and solution cavities, all contribute to wellbore instability in carbonate formation. Consequently, a meticulous survey of cracks and solution cavities is essential during the drilling design phase for carbonate formation. This survey should encompass the relationship between cracks and in situ stress, crack dip angle and width, solution cavity diameters and quantity, as well as the connectivity of cracks and solution cavities. A comprehensive analysis of the characteristics of cracks and solution cavities should then be integrated to evaluate the wellbore stability. Ultimately, this approach enables the development of a reliable drilling design that incorporates appropriate drilling fluid densities and excellent drilling fluid properties. Such a design is crucial for ensuring the safety of drilling operations in carbonate formation.

## 5. Conclusions

- (1) Cracks and solution cavities are prevalent in the Dengying Formation carbonate reservoir in the Gaoshiti–Moxi area of the Sichuan Basin. Horizontal cracks are the most predominant, followed by inclined cracks, with an average crack density ranging from 0.86 to 8.26 per meter. Additionally, there is a multitude of solution cavities, with an average development density of 26.45 per meter. The extensive development of cracks and solution cavities contributes to the discrete nature of the rock's mechanical parameters.
- (2) Taking into account the influence of cracks and solution cavities, the equivalent drilling fluid density for collapse pressure ( $\rho_c$ ) in the 5182–5187 m section of Well GS10 is determined to be 1.16 g/cm<sup>3</sup>. This represents a 6.42% increase compared to the value obtained without considering the effect of cracks and solution cavities, which aligns well with engineering practice. In addition, cracks play a more significant role than solution cavities in affecting the wellbore stability.
- (3) As the angle of the crack strike deviates further from the direction of maximum horizontal principal stress, stress and displacement at all points around the wellbore progressively increase, resulting in a linear increase in  $\rho_c$ . Similarly, as the dip angle and width of cracks increase, both stress and displacement at the intersection of cracks and the wellbore gradually intensify, leading to a linear increase in  $\rho_c$ .
- (4) As the solution cavities diameter ( $D$ ) increases, the stress and displacement at various points around the wellbore gradually intensify, and initially,  $\rho_c$  increases linearly.

However, when  $D$  exceeds 609 mm, there is no significant change in  $\rho_c$ . Additionally, as the number of solution cavities increases, both stress and displacement around the wellbore progressively rise, and  $\rho_c$  increases approximately in a linear trend.

- (5) The disturbed stress area around the wellbore increases by 45.23% when cracks and solution cavities are connected compared to when disconnected. Furthermore, the stress around the wellbore is higher when cracks and solution cavities are connected than when disconnected;  $\rho_c$  for the situation when cracks and solution cavities are connected increases by 13.33% compared to when disconnected.

**Author Contributions:** Conceptualization, Q.Z.; Methodology, J.Z. and R.Z.; Project administration, R.Z.; Validation, H.A.; Formal analysis, W.L. and Q.Z.; Investigation, J.Z. and Y.G.; Resources, R.Z. and X.F.; Data curation, R.Z. and W.L.; Writing—original draft, J.Z. and Y.G.; Writing—review and editing, H.A. and Q.Z.; Funding acquisition, X.F. and Q.Z.; Supervision, X.F. All authors have read and agreed to the published version of the manuscript.

**Funding:** This research was funded by the National Natural Science Foundation of China (Grant Nos. 42172313 and 51774246) and the Natural Science Foundation of Sichuan Province (Grant Nos. 2024NSFSC0203, 2022NSFSC0185 and 2023NSFSC0938).

**Institutional Review Board Statement:** Not applicable.

**Informed Consent Statement:** Not applicable.

**Data Availability Statement:** The data presented in this study are openly available in [Mendeley Data] at [<https://doi.org/10.17632/t6bmr8thbc.1>].

**Acknowledgments:** The authors would like to express their gratitude to the editors and anonymous reviewers for their constructive comments on the draft paper. The authors are also grateful to Xingyu Mou, Qianwen Mo, Kang Ding, Xiwei Wang, and Yang Feng for their contributions to data curation, investigation, and reviewing.

**Conflicts of Interest:** Jingzhe Zhang, Rongrong Zhao, Hongyi An and Wenhao Li are currently employed by CNPC Southwest Oil and Gas Field Company. Yuxin Geng is currently employed by CNPC Huabei Oil Field Company. The remaining authors declare that the research was conducted in the absence of any commercial or financial relationships that could be construed as a potential conflict of interest.

## References

- Zhang, Q.; Yao, B.; Fan, X.; Li, Y.; Fantuzzi, N.; Ma, T.; Chen, Y.; Zeng, F.; Li, X.; Wang, L. A failure criterion for shale considering the anisotropy and hydration based on the shear slide failure model. *Int. J. Min. Sci. Technol.* **2023**, *33*, 447–462. [[CrossRef](#)]
- Zhang, M.; Fan, X.; Zhang, Q.; Yang, B.; Zhao, P.; Yao, B.; He, L. Influence of multi-planes of weakness on unstable zones near wellbore wall in a fractured formation. *J. Nat. Gas Sci. Eng.* **2021**, *93*, 104026. [[CrossRef](#)]
- Hao, Y. Effect of stratum properties on wellbore stability. *Chem. Technol. Fuels Oil* **2015**, *51*, 556–563. [[CrossRef](#)]
- Allawi, R.H. Chemical and mechanical model to analysis wellbore stability. *Pet. Sci. Technol.* **2023**, *42*, 3062–3084. [[CrossRef](#)]
- Younessi, A.; Rasouli, V. A fracture sliding potential index for wellbore stability analysis. *Int. J. Rock Mech. Min.* **2010**, *47*, 927–939. [[CrossRef](#)]
- Qiu, Y.; Ma, T.; Peng, N.; Liu, Y.; Liu, J.; Ranjith, P.G. Wellbore stability analysis of inclined wells in transversely isotropic formations accounting for hydraulic-mechanical coupling. *Geoenergy Sci. Eng.* **2023**, *224*, 211615. [[CrossRef](#)]
- Zhang, Q.; Yan, Z.; Fan, X.; Li, Z.; Zhao, P.; Shuai, J.; Jia, L.; Liu, L. Field monitoring and identification method for overflow of fractured-vuggy carbonate reservoir. *Energies* **2023**, *16*, 2399. [[CrossRef](#)]
- Yang, X.; Liu, Z.; Zhang, H.; Xiong, Q.; Liu, H. An analysis on wellbore collapse of open hole completion in carbonate formation. *Appl. Mech. Mater.* **2012**, *220*, 220–223. [[CrossRef](#)]
- Martyushev, D.A.; Ponomareva, I.N.; Chukhlov, A.S.; Davoodi, S.; Osovetsky, B.M.; Kazymov, K.P.; Yang, Y.F. Study of void space structure and its influence on carbonate reservoir properties: X-ray microtomography, electron microscopy, and well testing. *Mar. Pet. Geol.* **2023**, *151*, 106192. [[CrossRef](#)]
- Li, W.Q.; Mu, L.; Zhao, L.; Li, J.; Wang, S.; Fan, Z.; Shao, D.; Li, C.; Shan, F.; Zhao, W.; et al. Pore-throat structure characteristics and its impact on the porosity and permeability relationship of Carboniferous carbonate reservoirs in eastern edge of Pre-Caspian Basin. *Pet. Explor. Dev.* **2020**, *47*, 1027–1041. [[CrossRef](#)]
- Liu, H.; Cui, S.; Men, Y.; Han, X. Dynamic analysis of wellbore stress field and wellbore stability in carbonate reservoir production process. *Arab. J. Geosci.* **2019**, *12*, 585. [[CrossRef](#)]

12. Liu, P.; Jiang, L.; Tang, B.; Ren, K.; Huang, M.; Geng, C. Residual oil distribution pattern in a fault-solution carbonate reservoir and countermeasures to improve oil development effectiveness. *Geofluids* **2022**, *2022*, 2147200. [[CrossRef](#)]
13. Ren, Q.; Jin, Q.; Feng, J.; Li, M. Simulation of stress fields and quantitative prediction of fractures distribution in upper Ordovician biological limestone formation within Hetianhe field, Tarim Basin, NW China. *J. Pet. Sci. Eng.* **2019**, *173*, 1236–1253. [[CrossRef](#)]
14. Sun, Y.; Cheng, Y.; Hao, Y.; Meng, M.; Dai, X.; Wang, Y.; Dong, S.; Peng, G. Analysis of borehole stability for inclined wells in fractured carbonate formation. *Fresen Environ. Bull.* **2019**, *28*, 3893–3899.
15. Liu, H.; Cui, S.; Meng, Y.; Han, X.; Liu, T.; Fan, Y.; Tao, Y.; Yu, A. A new method for wellbore stability evaluation based on fractured carbonate reservoir rock breaking degree. *Arab. J. Geosci.* **2021**, *14*, 647. [[CrossRef](#)]
16. Yan, X.; You, L.; Kang, Y.; Li, X.; Xu, C.; She, J. Impact of drilling fluids on friction coefficient of brittle gas shale. *Int. J. Rock Mech. Min.* **2018**, *106*, 144–152. [[CrossRef](#)]
17. Zhang, L.; Yan, X.; Yang, X.; Zhao, X. An analytical model of coal wellbore stability based on block limit equilibrium considering irregular distribution of cleats. *Int. J. Coal Geol.* **2015**, *152*, 147–158. [[CrossRef](#)]
18. Liu, H.; Liu, T.; Meng, Y.; Han, X.; Cui, S.; Yu, A. Experimental study and evaluation for borehole stability of fractured limestone formation. *J. Pet. Sci. Eng.* **2019**, *180*, 130–137. [[CrossRef](#)]
19. Karatela, E.; Taheri, A.; Xu, C.; Stevenson, G. Study on effect of in-situ stress ratio and discontinuities orientation on bore-hole stability in heavily fractured rocks using discrete element method. *J. Pet. Sci. Eng.* **2016**, *139*, 94–103. [[CrossRef](#)]
20. Cui, S.; Liu, H.; Meng, Y.; Zhang, Y.; Tao, Y.; Zhang, X. Study on fracture occurrence characteristics and wellbore stability of limestone formation. *J. Pet. Sci. Eng.* **2021**, *204*, 108783. [[CrossRef](#)]
21. Liu, J.; Ma, T.; Fu, J.; Peng, N.; Qiu, Y.; Liu, Y.; Gao, J. Fully coupled two-phase hydro-mechanical model for wellbore stability analysis in tight gas formations considering the variation of rock mechanical parameters. *Gas Sci. Eng.* **2023**, *115*, 205023. [[CrossRef](#)]
22. Zhang, Q.; Ran, J.; Fan, X.; Yang, B.; Zhao, P.; Chen, Y.; Huang, P.; Zhang, M.; He, L. Mechanical properties of basalt, tuff and breccia in the Permian system of Sichuan Basin after water absorption—implications for wellbore stability analysis. *Acta Geotech.* **2023**, *18*, 2059–2080. [[CrossRef](#)]
23. Andabily, Z.; Ebrahim, M. Management of Wellbore Stability by Controlling Physical and Chemical Properties of Drilling Muds. Ph.D. Dissertation, University of New South Wales, Kensington, Australia, 1997.
24. Akhtarmanesh, S.; Shahrabi, M.J.A.; Atashnezhad, A. Improvement of wellbore stability in shale using nanoparticles. *J. Pet. Sci. Eng.* **2013**, *112*, 290–295. [[CrossRef](#)]
25. Li, J.; Ma, Y.; Liu, Y.; Liu, Q. Numerical simulation for the effect of mud cake time-dependent properties on wellbore stability. *Rock Mech. Rock Eng.* **2024**, *57*, 581–596. [[CrossRef](#)]
26. Gholilou, A.; Far, P.B.; Vialle, S.; Madadi, M. Determination of safe mud window considering time-dependent variations of temperature and pore pressure: Analytical and numerical approaches. *J. Rock Mech. Geotech. Eng.* **2017**, *9*, 900–911. [[CrossRef](#)]
27. Gentzis, T.; Deisman, N.; Chalaturnyk, R.J. A method to predict geomechanical properties and model well stability in horizontal boreholes. *Int. J. Coal Geol.* **2009**, *78*, 149–160. [[CrossRef](#)]
28. Al-Ajmi, A.M.; Al-Harthy, M.H. Probabilistic wellbore collapse analysis. *J. Pet. Sci. Eng.* **2010**, *74*, 171–177. [[CrossRef](#)]
29. Al-Ajmi, A. Wellbore Stability Analysis Based on a New True-Triaxial Failure Criterion. Ph.D. Dissertation, KTH Royal Institute of Technology, Stockholm, Sweden, 2006.
30. Karatela, E.; Taheri, A. Three-dimensional hydro-mechanical model of borehole in fractured rock mass using discrete element method. *J. Nat. Gas Sci. Eng.* **2018**, *53*, 263–275. [[CrossRef](#)]
31. Guo, J.; She, C.; Liu, H.; Cui, S. Rock mechanical properties and wellbore stability of fractured dolomite formations. *ACS Omega* **2023**, *8*, 35152–35166. [[CrossRef](#)]
32. Liu, H.; Cui, S.; Meng, Y.; Han, Z.; Yang, M. Study on rock mechanical properties and wellbore stability of fractured carbonate formation based on fractal geometry. *ACS Omega* **2022**, *7*, 43022–43035. [[CrossRef](#)]
33. Gomar, M.; Goodarznia, I.; Shadizadeh, S.R. Transient thermo-poroelastic finite element analysis of borehole breakouts. *Int. J. Rock Mech. Min.* **2014**, *71*, 418–428. [[CrossRef](#)]
34. Zhao, W.; Wang, Z.; Jiang, H.; Fu, X.; Xie, W.; Xu, A.; Shen, A.; Shi, S.; Huang, S.; Jiang, Q. Exploration status of the deep Sinian strata in the Sichuan Basin: Formation conditions of old giant carbonate oil/gas fields. *Nat. Gas Ind. B* **2020**, *7*, 462–472. [[CrossRef](#)]
35. Zhou, L. Optimization and field application of reservoir stimulation of the Sinian Deng 4 member in the Sichuan Basin. *Nat. Gas Ind. B* **2022**, *9*, 277–288. [[CrossRef](#)]
36. Wang, L.; He, Y.; Peng, X.; Deng, H.; Liu, Y.; Xu, W. Pore structure characteristics of an ultradeep carbonate gas reservoir and their effects on gas storage and percolation capacities in the Deng IV member, Gaoshiti-Moxi Area, Sichuan Basin, SW China. *Mar. Pet. Geol.* **2020**, *111*, 44–65. [[CrossRef](#)]
37. DZ/T 0276.20–2015; Ministry of Land and Resources of the People’s Republic of China Regulation for the Physical and Mechanical Propertier of Rock—Part 20: Test for Determining the Strength of Rock in Triaxial Compression. Industry Standard of Geology and Mineral Resources of the People’s Republic of China: Beijing, China, 2015.
38. Zhang, Q.; Fan, X.; Chen, P.; Ma, T.; Zeng, F. Geomechanical behaviors of shale after water absorption considering the combined effect of anisotropy and hydration. *Eng. Geol.* **2020**, *269*, 105547. [[CrossRef](#)]
39. Fan, X.; Gong, M.; Zhang, Q.; Wang, J.; Bai, L.; Chen, Y. Prediction of the horizontal stress of the tight sandstone formation in eastern Sulige of China. *J. Pet. Sci. Eng.* **2014**, *113*, 72–80. [[CrossRef](#)]

- 
40. Fan, X.; Zhang, Q.; Duan, M.; Yang, Y.; Duan, Q.; Chen, X.; Lv, D. Mathematical model for calculating the horizontal principal stress of a faulted monoclinical structure in southwest Qaidam Basin, China. *AAPG Bull.* **2019**, *103*, 2697–2729. [[CrossRef](#)]

**Disclaimer/Publisher’s Note:** The statements, opinions and data contained in all publications are solely those of the individual author(s) and contributor(s) and not of MDPI and/or the editor(s). MDPI and/or the editor(s) disclaim responsibility for any injury to people or property resulting from any ideas, methods, instructions or products referred to in the content.